



HAL
open science

Age of the oldest known *Homo sapiens* from eastern Africa

Céline M Vidal, Christine S Lane, Asfawossen Asrat, Dan N Barfod, Darren F Mark, Emma L Tomlinson, Amdemichael Zafu Tadesse, Gezahegn Yirgu, Alan Deino, William Hutchison, et al.

► **To cite this version:**

Céline M Vidal, Christine S Lane, Asfawossen Asrat, Dan N Barfod, Darren F Mark, et al.. Age of the oldest known *Homo sapiens* from eastern Africa. *Nature*, 2022, 601, pp.579 - 583. 10.1038/s41586-021-04275-8. hal-03856390

HAL Id: hal-03856390

<https://hal.science/hal-03856390v1>

Submitted on 16 Nov 2022

HAL is a multi-disciplinary open access archive for the deposit and dissemination of scientific research documents, whether they are published or not. The documents may come from teaching and research institutions in France or abroad, or from public or private research centers.

L'archive ouverte pluridisciplinaire **HAL**, est destinée au dépôt et à la diffusion de documents scientifiques de niveau recherche, publiés ou non, émanant des établissements d'enseignement et de recherche français ou étrangers, des laboratoires publics ou privés.

Age of the oldest known *Homo sapiens* from eastern Africa

<https://doi.org/10.1038/s41586-021-04275-8>

Received: 29 March 2021

Accepted: 23 November 2021

Published online: 12 January 2022

Open access

 Check for updates

Céline M. Vidal^{1,2}✉, Christine S. Lane¹, Asfawossen Asrat^{3,4}, Dan N. Barfod⁵, Darren F. Mark⁵, Emma L. Tomlinson⁶, Amdemichael Zafu Tadesse⁷, Gezahegn Yirgu³, Alan Deino⁸, William Hutchison⁹, Aurélien Mounier^{10,11} & Clive Oppenheimer^{1,12}

Efforts to date the oldest modern human fossils in eastern Africa, from Omo-Kibish^{1–3} and Herto^{4,5} in Ethiopia, have drawn on a variety of chronometric evidence, including ⁴⁰Ar/³⁹Ar ages of stratigraphically associated tuffs. The ages that are generally reported for these fossils are around 197 thousand years (kyr) for the Kibish Omo I^{3,6,7}, and around 160–155 kyr for the Herto hominins^{5,8}. However, the stratigraphic relationships and tephra correlations that underpin these estimates have been challenged^{6,8}. Here we report geochemical analyses that link the Kamoya's Hominid Site (KHS) Tuff⁹, which conclusively overlies the member of the Omo-Kibish Formation that contains Omo I, with a major explosive eruption of Shala volcano in the Main Ethiopian Rift. By dating the proximal deposits of this eruption, we obtain a new minimum age for the Omo fossils of 233 ± 22 kyr. Contrary to previous arguments^{6,8}, we also show that the KHS Tuff does not correlate with another widespread tephra layer, the Waidedo Vitric Tuff, and therefore cannot anchor a minimum age for the Herto fossils. Shifting the age of the oldest known *Homo sapiens* fossils in eastern Africa to before around 200 thousand years ago is consistent with independent evidence for greater antiquity of the modern human lineage¹⁰.

Only eight sites in Africa have yielded possible early anatomically modern *Homo sapiens* fossils from the late Middle Pleistocene (approximately 350–130 thousand years ago (ka))¹¹. Most of these have considerable age uncertainty or debatable *H. sapiens* apomorphy¹¹. A principal method for constraining the fossil ages is the use of single-crystal ⁴⁰Ar/³⁹Ar isotope dating applied to stratigraphically associated volcanic ash (tephra) beds^{12–14}. However, many distal tephra deposits consist largely of glass and lack suitable crystals for dating. In this case, geochemical fingerprinting can be used to match a tephra layer to more readily dated proximal deposits with larger, more abundant phenocrysts. The most widely accepted fossils that are interpreted as possessing unequivocal modern cranial apomorphies (that is, a tall cranial vault and a chin) and classified as *H. sapiens* are two Ethiopian finds^{11,15,16}, namely the Omo I¹ and Herto specimens⁴. Accordingly, the evidence that constrains their ages assumes particular importance but is a topic of considerable geochronological controversy^{3,6,8}.

The Omo I remains were discovered in the late 1960s in the lower Omo valley of southern Ethiopia^{1,14}, at the surface of a siltstone near the top of Member I of the Omo-Kibish Formation (Fig. 1a, b). The maximum age of Omo I was derived from the ⁴⁰Ar/³⁹Ar age of 196 ± 4 kyr (2σ)^{3,6,17} obtained for alkali feldspar phenocrysts from the three youngest pumice clasts that were sampled from a heterogeneous tuffaceous

deposit correlated with the Nakaa'kire Tuff³, which is reported to lie “near, but probably slightly below” the fossils³ (Fig. 1b). Recalculated using a more widely adopted age of 28.201 million years (Myr) for the irradiation monitor (sanidine from the Fish Canyon Tuff of Colorado)¹⁸, the Nakaa'kire Tuff age shifts marginally to 197 ± 4 kyr. Owing to the uncertain stratigraphic relationship between this tuff and the hominin fossils¹⁹, much attention has been focused on dating the KHS Tuff—a widespread, more-than-2-m-thick deposit of fine ash fallout at the base of Member II of the Omo-Kibish Formation (Fig. 1b). The KHS Tuff overlies Member I, where Omo I was retrieved around 1.4 m lower down section, and is demonstrably younger than the fossils^{3,9}. Although the Nakaa'kire Tuff was identified in several sections below the KHS Tuff, the latter was not found in the same section from which the dated pumice clasts correlated with the Nakaa'kire Tuff (on the basis of major element composition) were sampled³. The fine grain size of the KHS Tuff has precluded direct ⁴⁰Ar/³⁹Ar dating, and no correlation to a source volcano or proximal pyroclastic unit has to our knowledge been made previously. However, drawing on published major element glass compositions, it has been correlated with both tephra TA-55^{20,21} from the Konso Formation and the directly ⁴⁰Ar/³⁹Ar-dated 184 ± 10 kyr unit D²² (recalculated age) of the Gademotta Formation⁶ (Fig. 1b). Relating the sediment flux in the Omo-Kibish basin with high lake levels that

¹Department of Geography, University of Cambridge, Cambridge, UK. ²Fitzwilliam College, University of Cambridge, Cambridge, UK. ³School of Earth Sciences, Addis Ababa University, Addis Ababa, Ethiopia. ⁴Department of Mining and Geological Engineering, Botswana International University of Science and Technology, Palapye, Botswana. ⁵NEIF Argon Isotopes, University of Glasgow, SUERC, Glasgow, UK. ⁶Trinity College Dublin, University of Dublin, Dublin, Ireland. ⁷Department of Geosciences, Environment and Society, Université Libre de Bruxelles, Brussels, Belgium. ⁸Berkeley Geochronology Center, Berkeley, CA, USA. ⁹School of Earth and Environmental Sciences, University of St Andrews, St Andrews, UK. ¹⁰Histoire Naturelle de l'Homme Préhistorique (HNHP, UMR 7194), MNHN/CNRS/UPVD, Musée de l'Homme, Paris, France. ¹¹Leverhulme Centre for Human Evolutionary Studies, Department of Archaeology, University of Cambridge, Cambridge, UK. ¹²McDonald Institute for Archaeological Research, Cambridge, UK. ✉e-mail: cv325@cam.ac.uk

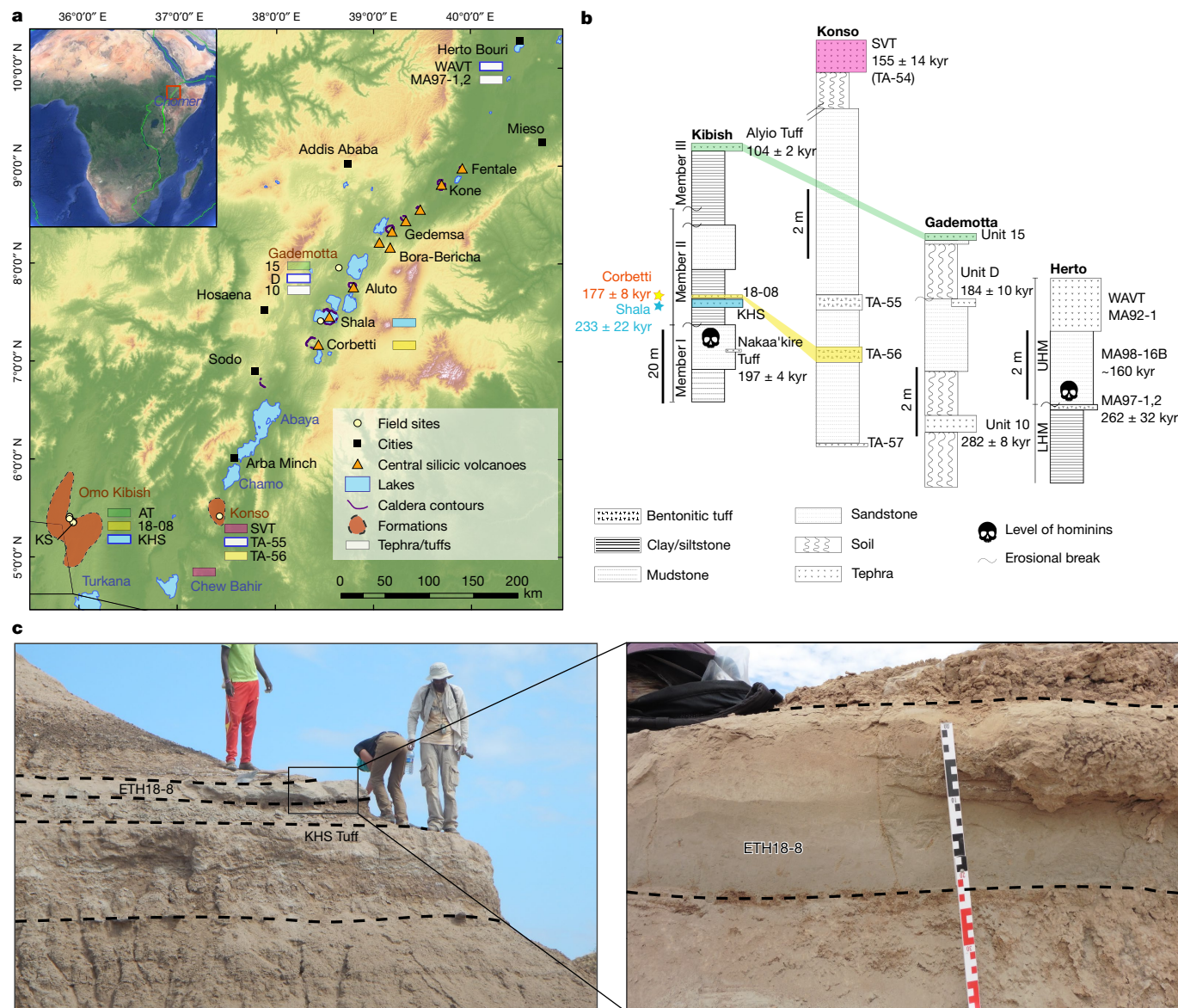


Fig. 1 | Late Middle Pleistocene tephrostratigraphy of the Main Ethiopian Rift. **a**, Map of the MER showing silicic volcanoes and the late Middle Pleistocene sedimentary formations and relevant tephra units. White boxes with blue edges depict former correlatives of the KHS Tuff^{6,8}. **b**, Synthetic stratigraphic logs of the late Middle Pleistocene formations showing former

correlations for the Alyio Tuff⁶ (green), Konso SVT (pink, also identified in the Chew Bahir sediment core³³), new correlations for Konso unit TA-56 (yellow), and source eruptions (stars). LHM, lower Herto Member; UHM, upper Herto Member. **c**, Tephra ETH18-8 above the KHS Tuff at the KS locality in the Omo-Kibish Formation⁹.

correspond to Mediterranean sapropel deposition^{9,23}, a slightly younger age for the KHS Tuff of around 172 kyr has also been proposed⁶. Either of these ages (184 or 172 kyr) would be consistent with the proposed age of 197 ± 4 kyr for Omo I.

The Herto *H. sapiens* fossils were recovered in the late 1990s in the Middle Awash^{4,5} (Afar rift; Fig. 1a). They were preserved in a sandstone within the upper Herto Member of the Bouri Formation (Fig. 1b). This sandstone is capped by the Waidedo Vitric Tuff (WAVT) (Fig. 1b), which is widespread across western Afar and is also present at Gona²⁴, 50 km north of Herto. Direct dating of the WAVT has remained inconclusive owing to crystal contamination, but dating of pumice and obsidian clasts in the fossiliferous sandstone yielded a maximum age of around 160 kyr (ref. ⁵). The WAVT was identified as a distal correlative of tephra TA-55 (Fig. 1b), on the basis of major element analysis of individual grains and major and trace element analysis of purified bulk separates^{5,25}. In Konso, unit TA-55 lies below the 155 ± 14 kyr Silver Tuff⁵ (SVT) (recalculated age) (Fig. 1b), suggesting an age for the Herto fossils of

around 160–155 kyr (ref. ⁴). This finding was challenged, however, in a study⁶ that correlated the Kibish KHS with Konso TA-55, and therefore with the Herto WAVT (Fig. 1b). This argument suggested an age of around 172 kyr for the WAVT, contradicting the established Herto stratigraphy. The Herto research group⁸ responded by corroborating their original stratigraphy, with the WAVT above the Herto fossils, thus challenging an age of about 172 kyr for the KHS. They concluded that the KHS, Konso unit TA-55⁵, Gademotta unit D (around 184 kyr)²² and WAVT⁵ could all represent a single tephrostratigraphic marker lying above the Omo-Kibish and Herto *H. sapiens* fossils, but that multiple eruptive sources would also be plausible⁸ (Fig. 1b). Given the lingering uncertainties of the stratigraphic relationship of the Naka'a'kire Tuff to Omo I, the age of the KHS Tuff becomes critical to the chronostratigraphy of these sites.

We have re-sampled the KHS Tuff and other pertinent ash deposits at Omo-Kibish, Konso and Gademotta to assess the geochemical correlations from which the ages of the oldest modern human fossils are

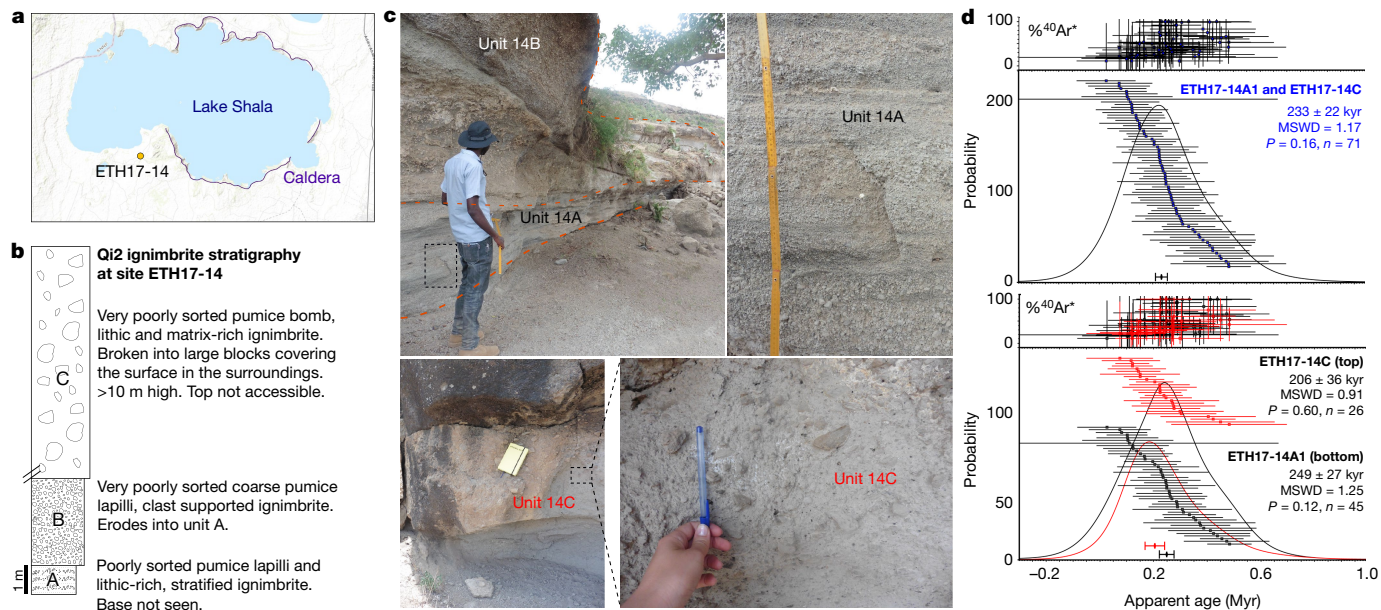


Fig. 2 | Stratigraphy and age of the Shala Qi2 ignimbrite. **a**, Location of site ETH17-14 near Lake Shala in the MER. **b**, Synthetic stratigraphy of the Qi2 ignimbrite of Shala at location ETH17-14. **c**, Photographs of units 14A, 14B and 14C of the Qi2 ignimbrite at site ETH17-14. Field observations indicate that deposits 14A and 14B are subunits of the same phase of the Qi2 eruption. **d**, $^{40}\text{Ar}/^{39}\text{Ar}$ age pooled data plotted on ideograms for samples 14A and 14C of

the Qi2 ignimbrite (bottom) yielding a preferred composite eruption age of 233 ± 22 kyr (top). Data are weighted means. Error bars show data and results at 2σ . $^{40}\text{Ar}^*$, radiogenic ^{40}Ar ; MSWD, mean square of weighted deviates; P , probability that residuals are explained by measurement errors exclusively; n , number of accepted grains.

inferred. While revisiting the sampling locality of the KHS Tuff (KS type section)⁹ at Omo-Kibish, we sampled another tephra layer in Member II (Fig. 1c) in an outcrop about 100 m from the KS type section. Unit ETH18-8 is an approximately 15-cm-thick, very well-sorted crystal-rich fine sand grey tephra layer situated 40 cm above the KHS Tuff (Fig. 1c). It is ubiquitous between the KHS section (KS) and the Chibele section (CB), and might stratigraphically correspond to unit CRF-23 previously identified above the KHS Tuff at the CB section⁹, although this cannot be confirmed through geochemical analysis because of the different microprobe conditions used.

In an attempt to identify and date the eruption that generated the KHS tuff, we included samples of ignimbrites from the caldera-forming eruptions of Shala and Corbetti volcanoes. Shala and Corbetti are the only Main Ethiopian Rift (MER) systems known to have produced major eruptions between around 170 ka and 250 ka²⁶. At Shala, the largest caldera in the central MER (Fig. 2a), we sampled at a more-than-20-m-thick exposure of the unwelded Qi2 ignimbrite²⁷ (Fig. 2b, c), southwest of Lake Shala and 350 km northeast of Omo-Kibish (Fig. 2a). We also analysed glass from a welded ignimbrite (COI2E) attributed to the formation of Corbetti caldera, dated at 177 ± 8 kyr (ref. ²⁶). A challenge of geochemical correlations between proximal and distal tephra deposits in the region is similarity in major and trace element compositions between pyroclastic products, not only of the same volcano but of different volcanoes in the MER²⁸. Accordingly, correlations are ideally based on a detailed suite of major, minor and trace element single-grain glass shard or pumice glass analyses.

The KHS glass shards are homogeneous pantelleritic rhyolite in composition (77.0 ± 0.3 wt% SiO_2 , 9.7 ± 0.1 wt% Al_2O_3 , 5.0 ± 0.1 wt% FeO^* (FeO^* refers to the total Fe as FeO) and 7.1 ± 0.4 wt% $\text{Na}_2\text{O} + \text{K}_2\text{O}$; Supplementary Table 1). Immobile oxide abundances, including FeO^* , CaO , Al_2O_3 and TiO_2 (Fig. 3, Supplementary Table 1), correspond with those of glasses from the proximal products of the Qi2 eruption of Shala volcano (samples ETH17-14A1, B1, B5 and C) (Figs. 2b, c, 3, Supplementary Fig. 4, Supplementary Table 1, Supplementary Information). These correlations are corroborated by comparing immobile

trace element ratios for Qi2 and KHS glasses and principal component analysis (Fig. 3, Supplementary Figs. 4, 5, Supplementary Table 2, Supplementary Information).

In addition, we find that the COI2E pantelleritic rhyolite glass from the 177 ± 8 kyr (ref. ²⁶) Corbetti ignimbrite (74.3 ± 0.2 wt% SiO_2 , 9.1 ± 0.1 wt% Al_2O_3 , 5.6 ± 0.2 wt% FeO^* and 10.1 ± 0.2 wt% $\text{Na}_2\text{O} + \text{K}_2\text{O}$) (Fig. 3, Supplementary Fig. 4, Supplementary Table 1, Supplementary Information) has immobile oxides and trace element abundances that match those for Kibish unit ETH18-8 and Konso TA-56 (Fig. 3, Supplementary Figs. 4, 5, Supplementary Table 2, Supplementary Information).

We used the $^{40}\text{Ar}/^{39}\text{Ar}$ dating method to analyse 113 individual sanidine crystals extracted from pumice samples ETH17-14A1 (base, 68 crystals) and ETH17-14C (top, 45 crystals) collected from the Shala Qi2 deposits (Fig. 2). The resulting data were filtered to exclude grains with low gas yields, at or below blank level, and xenocrysts with ages significantly older than the mean of the dataset (six grains with ages exceeding 1 Myr). The distributions of ages from each sample were indistinguishable at 2σ uncertainty (Fig. 2d). Combining analyses from both pumice samples yielded a weighted mean of 233 ± 22 kyr at 2σ (Fig. 2d, Supplementary Table 3), thereby dating the Qi2 eruption and the KHS tuff.

An age of 233 ± 22 kyr for KHS is consistent with the 177 ± 8 kyr age that we associate with the overlying ETH18-8 tephra (Fig. 1b). However, it casts doubt on the suggested correlation between high deposition fluxes in the Omo basin with large in-flows of fresh water from the Nile River system into the Mediterranean sea^{6,7,9}, at least during the formation of Member II. Our KHS age is incongruent with the formation of Mediterranean Sapropel S6 at 172 ka⁶, and instead overlaps the timing of the formation of sapropel S8 (217 ka)^{9,29}. Although the 177 ± 8 kyr age of ETH18-8 is consistent with the formation of sapropel S6 (172 ka)²⁹, only a mudstone unit of around 40 cm thickness separates KHS from ETH18-8, which cannot account for the suggested rapid deposition in the basin concomitant with sapropel S7 (192–199 ka)³.

The revised Omo-Kibish stratigraphy is also incompatible with the 197 ± 4 kyr age reported for the Nakaa'kire Tuff^{3,7,9}, which is found in

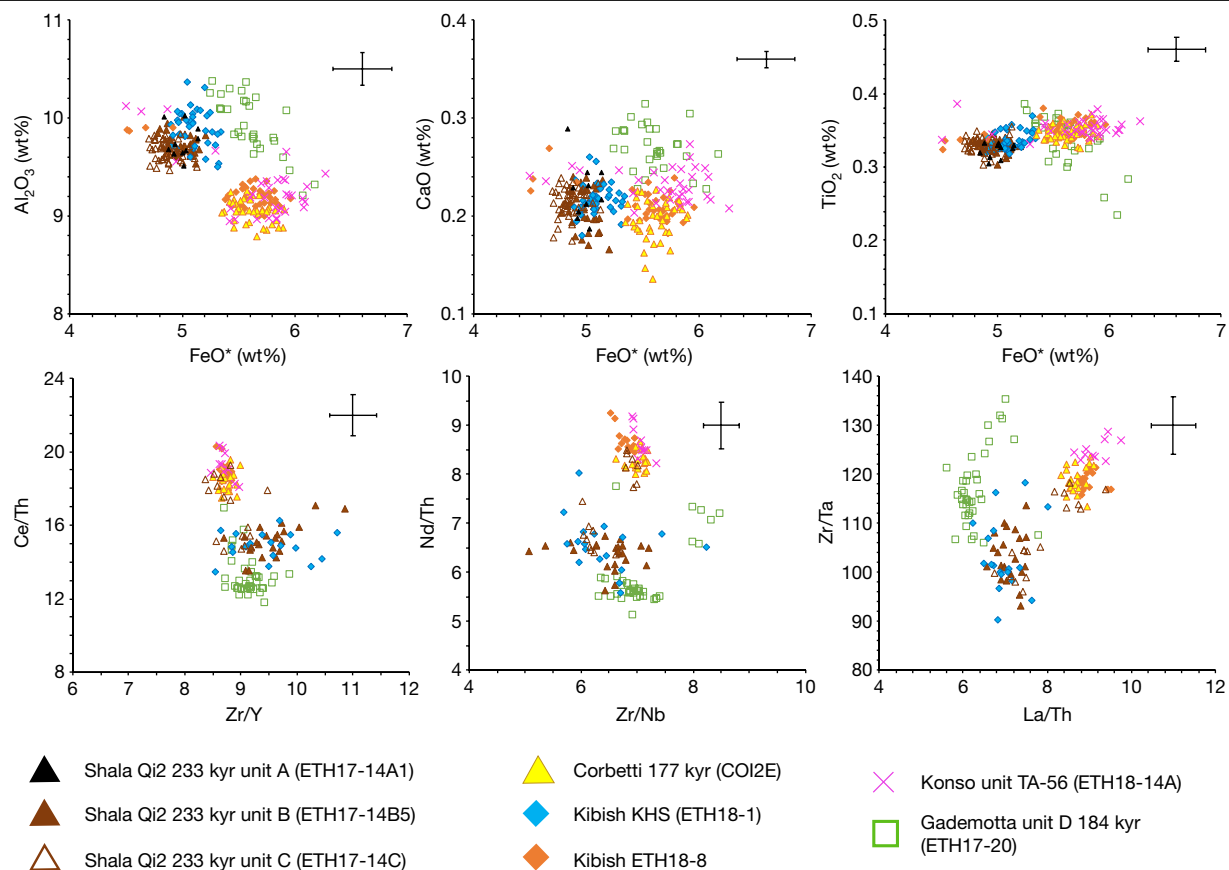


Fig. 3 | Geochemical fingerprints of MER tephra and their sources.

Major element abundances and trace element ratios of glasses from the Shala Qi2 ignimbrite (around 233 kyr), the Corbetti ignimbrite (around 177 kyr), the Gademotta unit D (around 184 kyr), the Kibish KHS and ETH18-8 tuffs, and the Konso TA-56 tuffs (all data from this study). Major element data are normalized to 100% anhydrous. Error bars shown are relative standard deviations derived from repeat measurements of matrix match glass

secondary standards STH-S6 (for FeO*, $n = 91$; Supplementary Table 6) and ATHO-G (for Al₂O₃, CaO and TiO₂, $n = 70$; Supplementary Table 6). They are plotted in the top right corner of each plot for clarity and rescaled to the value of the centre point. In the case of element ratios, error propagation has been applied using analyses of standard ATHO-G ($n = 15$; Supplementary Table 7). Additional compositional observations and biplots are presented in Supplementary Fig. 5.

Member I of the formation^{3,7,9} and which must therefore be older than 233 ± 22 kyr. The age of 197 ± 4 kyr was inferred from three out of five dated pumice clasts from lenses found in ‘a sandy tuffaceous matrix’⁷. Although these samples had similar major element compositions to the Nakaa’kire Tuff, they were collected from a lateral outcrop and not in section^{3,7,9}. Given the uncertainty in the age and stratigraphic placement of the Nakaa’kire Tuff, as well as its heterogeneous lithology and geochemistry, the identification of the 233 ± 22 ka Qi2 eruption of Shala as the source of the KHS Tuff provides a more robust minimum age for Omo I *H. sapiens*.

Furthermore, our glass compositional data, source correlation and age estimate for KHS allow us to re-assess its identification at other archaeological sites in Ethiopia. New lithological examination of the pedogenically altered unit TA-55 at Konso (Supplementary Fig. 1) in grain size fractions of greater than $125 \mu\text{m}$, greater than $80 \mu\text{m}$ and greater than $25 \mu\text{m}$, after density separation, failed to identify glass shards in this deposit, which was previously correlated with the WAVT at Herto. This precluded evaluation of the reported correlation with the KHS Tuff⁶. However, with the underlying unit TA-56 now correlated with Kibish unit ETH18-8 and the 177 ± 8 kyr Corbetti ignimbrite (Fig. 3, Supplementary Figs. 4, 5), it is clear that TA-55 is younger than 177 ± 8 kyr and so cannot correlate with Qi2 or the KHS Tuff.

Although the 184 ± 10 kyr unit D of Gademotta appears close to KHS in major element contents, neither major nor trace element abundances clearly overlap (Fig. 3, Supplementary Figs. 4, 5, Supplementary Information), precluding a match. Immobile trace element ratios and

principal component analysis show that unit D also differs from TA-56 (Fig. 3, Supplementary Figs. 4, 5, Supplementary Information).

The correlation of the Herto WAVT with Konso unit TA-55⁵, around 800 km south of Herto, led earlier investigators to accept the 155 ± 14 kyr age of the SVT at Konso as the *terminus ante quem* of the Herto fossils. This correlation has been debated³⁰ but reinforced by additional geochemical data²⁵. We were unable to find preserved glass in our TA-55 sample but our results undermine the tephrostratigraphic correlations proposed between the Omo-Kibish, Gademotta and Konso formations⁶ and bracket the age of the Konso TA-55 tuff between 177 ± 8 kyr (TA-56) and 155 ± 14 kyr (SVT). Although its correlation with the WAVT at Herto should be confirmed in the future using grain-discrete single-point glass analyses, this age bracket is consistent with the underlying Herto fossiliferous sandstone (approximately 160 kyr)⁵, and confirms that the Herto *H. sapiens* fossils are considerably younger than Omo I at Omo-Kibish.

Our new age constraints are congruent with most models for the evolution of modern humans, which estimate the origin of *H. sapiens* and its divergence from archaic humans at around 350–200 ka (refs. ^{16,31,32}). The challenge remains to obtain a robust maximum age for Omo I. Our revised tephrostratigraphy demonstrates that the Herto specimens postdate the Omo I remains from Omo-Kibish, and that they do not lie beneath the same tephra horizon as the Kibish fossils, as previously inferred⁸. Further geochemical data are needed to clarify the relationship between the WAVT and other MER tephra, and may ultimately identify the WAVT source, promising a more reliable

minimum age for the Herto fossils. More generally, continued efforts to develop the tephrochronological framework for eastern Africa will help in addressing a range of interrelated volcanological, palaeoenvironmental and palaeoanthropological questions.

Online content

Any methods, additional references, Nature Research reporting summaries, source data, extended data, supplementary information, acknowledgements, peer review information; details of author contributions and competing interests; and statements of data and code availability are available at <https://doi.org/10.1038/s41586-021-04275-8>.

1. Day, M. H. Early *Homo sapiens* remains from the Omo River region of South-west Ethiopia: Omo human skeletal remains. *Nature* **222**, 1135–1138 (1969).
2. Fleagle, J. G., Assefa, Z., Brown, F. H. & Shea, J. J. Paleoanthropology of the Kibish Formation, southern Ethiopia: introduction. *J. Hum. Evol.* **55**, 360–365 (2008).
3. McDougall, I., Brown, F. H. & Fleagle, J. G. Stratigraphic placement and age of modern humans from Kibish, Ethiopia. *Nature* **433**, 733–736 (2005).
4. White, T. D. et al. Pleistocene *Homo sapiens* from Middle Awash, Ethiopia. *Nature* **423**, 742–747 (2003).
5. Clark, J. D. et al. Stratigraphic, chronological and behavioural contexts of Pleistocene *Homo sapiens* from Middle Awash, Ethiopia. *Nature* **423**, 747–752 (2003).
6. Brown, F. H., McDougall, I. & Fleagle, J. G. Correlation of the KHS Tuff of the Kibish Formation to volcanic ash layers at other sites, and the age of early *Homo sapiens* (Omo I and Omo II). *J. Hum. Evol.* **63**, 577–585 (2012).
7. McDougall, I., Brown, F. H. & Fleagle, J. G. Sapropels and the age of hominins Omo I and II, Kibish, Ethiopia. *J. Hum. Evol.* **55**, 409–420 (2008).
8. Sahle, Y. et al. in *Modern Human Origins and Dispersal* (eds Sahle, Y. et al.) 73–104 (2019).
9. Brown, F. H. & Fuller, C. R. Stratigraphy and tephra of the Kibish Formation, southwestern Ethiopia. *J. Hum. Evol.* **55**, 366–403 (2008).
10. Richter, D. et al. The age of the hominin fossils from Jebel Irhoud, Morocco, and the origins of the Middle Stone Age. *Nature* **546**, 293–296 (2017).
11. Mounier, A. & Mirazón Lahr, M. Deciphering African late middle Pleistocene hominin diversity and the origin of our species. *Nat. Commun.* **10**, 3406 (2019).
12. Lane, C. S., Lowe, D. J., Blockley, S. P. E., Suzuki, T. & Smith, V. C. Advancing tephrochronology as a global dating tool: applications in volcanology, archaeology, and palaeoclimatic research. *Quat. Geochronol.* **40**, 1–7 (2017).
13. Abbott, P., Jensen, B. J. L. & Lowe, D. J. Crossing new frontiers: extending tephrochronology as a global geoscientific research tool. *J. Quat. Sci.* **35**, 1–8 (2020).
14. Lowe, D. J. Tephrochronology and its application: a review. *Quat. Geochronol.* **6**, 107–153 (2011).
15. Mirazón Lahr, M. The shaping of human diversity: filters, boundaries and transitions. *Phil. Trans. R. Soc. B* **371**, 20150241 (2016).
16. Stringer, C. The origin and evolution of *Homo sapiens*. *Phil. Trans. R. Soc. B* **371**, 20150237 (2016).
17. Butzer, K. W. & Thurber, D. L. Some Late Cenozoic sedimentary formations of the lower Omo Basin. *Nature* **222**, 1138–1143 (1969).
18. Kuiper, K. F. et al. Synchronizing rock clocks of earth history. *Science* **320**, 500–504 (2008).
19. Fleagle, J., Assefa, Z., Brown, F. & Shea, J. J. Paleoanthropology of the Kibish Formation, southern Ethiopia: introduction. *J. Hum. Evol.* **55**, 360–365 (2008).
20. Nagaoka, S. et al. Lithostratigraphy and sedimentary environments of the hominid-bearing Pliocene–Pleistocene Konso Formation in the southern Main Ethiopian Rift, Ethiopia. *Palaeogeogr. Palaeoclimatol. Palaeoecol.* **216**, 333–357 (2005).
21. Katoh, S. et al. Chronostratigraphy and correlation of the Plio–Pleistocene tephra layers of the Konso Formation, southern Main Ethiopian Rift, Ethiopia. *Quat. Sci. Rev.* **19**, 1305–1317 (2000).
22. Morgan, L. & Renne, P. Diachronous dawn of Africa’s Middle Stone Age: new ⁴⁰Ar/³⁹Ar ages from the Ethiopian Rift. *Geology* **36**, 967–970 (2008).
23. Rossignol-Strick, M. Mediterranean Quaternary sapropels, an immediate response of the African monsoon to variation of insolation. *Palaeogeogr. Palaeoclimatol. Palaeoecol.* **49**, 237–263 (1985).
24. Quade, J. et al. The geology of Gona. *Geol. Soc. Am. Bull.* **446**, 1–31 (2008).
25. Hart, W. K. et al. Dating of the Herto hominin fossils. *Nature* **426**, 622–622 (2003).
26. Hutchison, W. et al. A pulse of mid-Pleistocene rift volcanism in Ethiopia at the dawn of modern humans. *Nat. Commun.* **7**, 13192 (2016).
27. Mohr, P., Mitchell, J. G. & Reynolds, R. G. H. Quaternary volcanism and faulting at OA caldera, central Ethiopian rift. *Bull. Volcanol.* **43**, 173–189 (1980).
28. Fontijn, K. et al. Contrasting styles of post-caldera volcanism along the Main Ethiopian Rift: implications for contemporary volcanic hazards. *J. Volcanol. Geotherm. Res.* **356**, 90–113 (2018).
29. Kroon, D. et al. Oxygen isotope and sapropel stratigraphy in the Eastern Mediterranean during the last 3.2 million years. *Proc. Ocean Drill. Prog. Sci. Results* **160**, 181–189 (1998).
30. Faupl, P., Richter, W. & Urbanek, C. Geochronology: dating of the Herto hominin fossils. *Nature* **426**, 621–622 (2003).
31. Bergström, A., Stringer, C., Hajdinjak, M., Scerri, E. M. L. & Skoglund, P. Origins of modern human ancestry. *Nature* **590**, 229–237 (2021).
32. Schlebusch, C. M. et al. Southern African ancient genomes estimate modern human divergence to 350,000 to 260,000 years ago. *Science* **358**, 652–655 (2017).
33. Roberts, H. M. et al. Using multiple chronometers to establish a long, directly-dated lacustrine record: constraining more than 600,000 years of environmental change at Chew Bahir, Ethiopia. *Quat. Sci. Rev.* **266**, 107025 (2021).

Publisher’s note Springer Nature remains neutral with regard to jurisdictional claims in published maps and institutional affiliations.



Open Access This article is licensed under a Creative Commons Attribution 4.0 International License, which permits use, sharing, adaptation, distribution and reproduction in any medium or format, as long as you give appropriate credit to the original author(s) and the source, provide a link to the Creative Commons license, and indicate if changes were made. The images or other third party material in this article are included in the article’s Creative Commons license, unless indicated otherwise in a credit line to the material. If material is not included in the article’s Creative Commons license and your intended use is not permitted by statutory regulation or exceeds the permitted use, you will need to obtain permission directly from the copyright holder. To view a copy of this license, visit <http://creativecommons.org/licenses/by/4.0/>.

© The Author(s) 2022

Methods

Sampling

Stratigraphic descriptions and sampling were carried out during two field seasons in 2017 and 2018. We sampled the previously described²⁷ Qi2 eruption of Shala volcano, and we revisited the Konso^{20,21}, Omo-Kibish^{3,6,9} and Gademotta^{22,34} formations (Fig. 1). At each site we described extensively the stratigraphy of the outcrops, measured the thickness of units and sampled deposits where best exposed and least altered.

⁴⁰Ar/³⁹Ar dating

Feldspars were extracted from pumice samples at the Departments of Geography and Earth Sciences, University of Cambridge. Rocks were crushed in a jaw crusher and sieved to obtain a 250–500- μm size fraction, cleaned under water and passed through a Frantz magnetic barrier laboratory separator to isolate sanidine phenocrysts from the ground-mass. Because separates would still contain other phases (primarily glass and quartz), 100–200 sanidine grains were further handpicked and then leached in 5% HF to remove any glass attached to the crystals.

Samples and neutron flux monitors were packaged in copper foil and stacked in quartz tubes with the relative positions of packets precisely measured for later reconstruction of neutron flux gradients. The sample package was irradiated for 2 h in the Oregon State University reactor, Cd-shielded facility (CLICIT). Fish Canyon sanidine (28.294 ± 0.036 (1 σ) million years ago; Ma) (ref. ³⁵) was used to monitor ³⁹Ar production and establish neutron flux values (J) for the samples (Supplementary Table 4). Gas was extracted from samples via step-heating using a mid-infrared (10.6 μm) CO₂ laser with a non-gaussian, uniform energy profile and a 1.5-mm beam diameter. The samples were housed in a doubly pumped ZnS-window laser cell and loaded into a stainless steel planchette containing 208 2.0-mm-diameter round wells. Liberated argon was purified of active gases—for example, CO₂, H₂O, H₂, N₂ and CH₄—using three Zr-Al getters; one at 16 °C and two at 400 °C. Data were collected on a Mass Analyser Products MAP-215-50 single-collector mass spectrometer using an electron multiplier collector in dynamic collection (peak hopping) mode. Time-intensity data were regressed to inlet time with second-order polynomial or linear fits to the data. Sample runs were corrected using the standard deviation of blanks throughout the runs. Mass discrimination was monitored on a daily basis, between and within sample runs by analysis of an air standard aliquot delivered by an automated pipette system (see Supplementary Table 4 for D values). All blank, interference and mass discrimination calculations were performed with the MassSpec software package (MassSpec, v.8.058, A. Deino, Berkeley Geochronology Center). Decay constants and corrections (Supplementary Table 5) were made using the approach of Renne et al. 2010³⁶ with the parameters of Renne et al. 2011³⁵.

Following the approach of Kuiper et al. ¹⁸, samples with low radiogenic yields (⁴⁰Ar* < 10%, 23 grains), and obvious outliers (age > 1 Myr, 6 grains) were rejected. After this initial filtering, peak age distributions were defined by determining the youngest population of individual grain analyses ($n \geq 10$) that conforms to a Gaussian distribution with the expected scatter as indicated by the value of the mean square of weighted deviates (MSWD); this second stage of filtering resulted in the rejection of an additional ten older grains, leaving 71 accepted grains.

Ages for unit samples ETH17-14A1 and ETH17-14C are reported with two sigma errors in Supplementary Table 3 with the raw data in Supplementary Table 4. These two sub-samples from the top and bottom of the same stratigraphic unit are indistinguishable in age at 2σ uncertainty, which permits them to be combined into a single composite sample. The accepted age for this population is 234 ± 22 kyr (relative to ref. ³⁶) or 233 ± 22 kyr (relative to ref. ¹⁸). An inverse isochron plotted through the data (Supplementary Fig. 2) yields an age of 219 ± 27 kyr (⁴⁰Ar/³⁶Ar₀ = 314 ± 24 , MSWD = 1.1, $P = 0.19$, $n = 71$), which is indistinguishable from the accepted age.

Although we are using the Kuiper et al. (ref. ¹⁸) calibration, the Renne et al. 2011 (ref. ³⁶) calibration has quantifiable uncertainties and is our preferred age for the sample. Nevertheless, for consistency with previous work, the latter age (233 ± 22 kyr) is used throughout the manuscript.

Sample preparation for geochemical analyses

Sample preparation was carried out in the Cambridge Tephra Laboratory in line with the protocols of the International Focus Group on Tephrochronology (INTAV)^{12,37} for geochemical characterization of volcanic glass. Pumice samples of the Qi2 Shala eruption were crushed, sieved at 500, 250, and 125 μm , and washed in purified water and hydrochloric acid (1%) in an ultrasonic bath. Glass grains from the 125–250- μm fraction were handpicked under microscope, mounted in epoxy resin stubs, then sectioned and polished. Distal tephra samples from Gademotta (unit D), Konso (TA-55/ETH18-14B and TA-56/ETH18-14A) and Omo-Kibish formations (KHS, ETH18-08) were washed through a sieve in purified water at 80 or 25 μm , then dried, described under microscope and mounted in epoxy resin stubs, then sectioned and polished. Strongly altered samples of TA-56 (ETH18-14A) and TA-55 (ETH18-14B) units from the Konso formation were density extracted to facilitate the search for volcanic glass^{38,39}. Sample ETH18-14B from TA-55 was sieved at 125, 80 and 25 μm and residues inspected under the microscope, yet no glass was found.

Major element analysis

Mounted samples were analysed for major element compositions with a SX100 CAMECA electron microprobe at the Department of Earth Sciences, University of Cambridge. Major elements were measured with an accelerating voltage of 10 kV and a 10-nA defocused beam. Elements were counted on-peak for 10 s (Na, Si), 20 s (Al, Fe and K), 60 s (Ti, Mg, Ca, and Cl), 90 s (P) and 120 s (Mn). Sodium was measured first to minimize alkali loss. The analytical accuracy was checked against international standards ATHO-G, STH-S6 and internal peralkaline obsidian from Lipari (74 wt% SiO₂, 3.8 wt% Na₂O and 5.3 wt% K₂O). Replicate standard analyses and standard deviations are reported in Supplementary Table 6. The latter are used for error bars on biplots instead of the standard deviation of each sample, which is affected by their natural variability. Where possible, we analysed 40–50 points per sample. All analyses are reported in Supplementary Table 1.

Trace element analysis

Trace element compositions of individual tephra shards were analysed by laser ablation inductively coupled plasma mass spectrometry (LA-ICP-MS) at the iCRAG laboratory at Trinity College Dublin. The instrument used was a Thermo iCAPQ coupled to a Photon Machines 193-nm G2 laser and a Helex two-volume cell. We used a spot size of 40 μm , depending on the area available for analysis, a repetition rate of 6 Hz and a count time of 33 s (200 pulses) on the sample and 30 s on the gas blank (background). We analysed large-enough glass shards analysed by electron microprobe analysis (EMPA) for major elements; however, spots are not tied through codes as we used the average Ca concentration of each sample as Ca correction factor. Concentrations were calibrated using NIST 612 with ²⁹Si as the internal standard. Data reduction was undertaken in Iolite v.3.4 and a secondary Ca correction factor was applied⁴⁰. Accuracies of ATHO-G and StHs6/80-G MPI-DING glass analyses are typically better than 6% for most elements. The precision is reflected by the standard deviations of replicate standard analyses (Supplementary Table 7), used for error bars on Fig. 3, Supplementary Fig. 4. Standard deviations of trace element ratios (Fig. 3) take into account error propagation. Detailed compositions of samples are reported in Supplementary Table 2.

Reporting summary

Further information on research design is available in the Nature Research Reporting Summary linked to this paper.

Data availability

All data supporting the findings of this study are available within the paper and its Supplementary Information files. Background maps for Fig. 1 are Shuttle Radar Topography Mission Digital Elevation Model data at one arcsecond resolution from the NASA Land Processes Distributed Active Archive Center (<https://earthexplorer.usgs.gov/>); settlements, lakes and other features are from (<https://www.naturalearthdata.com/>). Background image for the top left corner inset of Fig. 1 from Google Earth and plate boundaries data courtesy of the US Geological Survey.

34. Laury, R. L. & Albritton, C. C. Geology of Middle Stone Age archaeological sites in the main Ethiopian Rift Valley. *Geol. Soc. Am. Bull.* **86**, 999–1011 (1975).
35. Renne, P. R., Balco, G., Ludwig, K. R., Mundil, R. & Min, K. Response to the comment by W.H. Schwarz et al. on ‘Joint determination of ^{40}K decay constants and $^{40}\text{Ar}^*/^{39}\text{K}$ for the Fish Canyon sanidine standard, and improved accuracy for $^{40}\text{Ar}/^{39}\text{Ar}$ geochronology’ by P.R. Renne et al. (2010). *Geochim. Cosmochim. Acta* **75**, 5097–5100 (2011).
36. Renne, P. R., Mundil, R., Balco, G., Min, K. & Ludwig, K. R. Joint determination of ^{40}K decay constants and $^{40}\text{Ar}^*/^{39}\text{K}$ for the Fish Canyon sanidine standard, and improved accuracy for $^{40}\text{Ar}/^{39}\text{Ar}$ geochronology. *Geochim. Cosmochim. Acta* **74**, 5349–5367 (2010).
37. Lowe, D. J. et al. Correlating tephra and cryptotephra using glass compositional analyses and numerical and statistical methods: review and evaluation. *Quat. Sci. Rev.* **175**, 1–44 (2017).
38. Blockley, S. P. E. et al. A new and less destructive laboratory procedure for the physical separation of distal glass tephra shards from sediments. *Quat. Sci. Rev.* **24**, 1952–1960 (2005).
39. Lane, C. S., Cullen, V. L., White, D., Bramham-Law, C. W. F. & Smith, V. C. Cryptotephra as a dating and correlation tool in archaeology. *J. Archaeol. Sci.* **42**, 42–50 (2014).
40. Tomlinson, E. L., Thordarson, T., Müller, W., Thirlwall, M. & Menzies, M. A. Microanalysis of tephra by LA-ICP-MS—strategies, advantages and limitations assessed using the Thorsmörk ignimbrite (Southern Iceland). *Chem. Geol.* **279**, 73–89 (2010).

Acknowledgements This study was supported by the Leverhulme Trust (‘Nature and impacts of Middle Pleistocene volcanism in the Ethiopian Rift’, 2016–21) and the Cambridge-Africa ALBORADA Research Fund (‘Volcanic tie-lines between records of past climates and early modern humans in Ethiopia, 2019–21’). Ar-Ar dating was supported by grant NIGFSC IP-1683-1116 through the UK Natural Environment Research Council. The iCRAG LA-ICP-MS facility at Trinity College Dublin is supported by SFI award 13/RC/2092. We acknowledge the local and regional authorities in Ethiopia for facilitating fieldwork and sample export, including the School of Earth Sciences Addis Ababa University, the Oromiya Regional State, the Ngangatom Woreda Local Administration and the FDRE Ministry of Mines, Petroleum and Natural Gas. We are grateful to Y. Beyene for assistance in accessing the Konso tephra localities; Ethioder and their drivers for logistical support; and field assistants Alex in Omo-Kibish and Demelash in Konso. We thank D. Colby for facilitating access to the Corbetti sample and A. Piermattei, I. Buisman and J. Day for assistance with sample preparation and microprobe analyses in Cambridge. The manuscript has benefited from comments by W. Hart and C. Feibel, and we are grateful to them for their input.

Author contributions C.M.V., C.O., C.S.L., A.A. and W.H. designed the study. C.M.V. and C.S.L. designed and conducted field and laboratory work and acquired, analysed and interpreted stratigraphic and geochemical data. A.A., G.Y., A.Z.T. and A.D. designed fieldwork and acquired and interpreted stratigraphic data in the field. D.N.B. and D.F.M. analysed and interpreted radiometric data. E.L.T. analysed samples for trace elements. A.M. contributed to palaeoanthropological discussion of the manuscript. All authors contributed to preparation and revision of the manuscript and approved the submitted version.

Competing interests The authors declare no competing or financial interests.

Additional information

Supplementary information The online version contains supplementary material available at <https://doi.org/10.1038/s41586-021-04275-8>.

Correspondence and requests for materials should be addressed to Céline M. Vidal.

Peer review information *Nature* thanks Craig Feibel, William Hart and the other, anonymous, reviewer(s) for their contribution to the peer review of this work.

Reprints and permissions information is available at <http://www.nature.com/reprints>.

Reporting Summary

Nature Portfolio wishes to improve the reproducibility of the work that we publish. This form provides structure for consistency and transparency in reporting. For further information on Nature Portfolio policies, see our [Editorial Policies](#) and the [Editorial Policy Checklist](#).

Statistics

For all statistical analyses, confirm that the following items are present in the figure legend, table legend, main text, or Methods section.

n/a Confirmed

- The exact sample size (n) for each experimental group/condition, given as a discrete number and unit of measurement
- A statement on whether measurements were taken from distinct samples or whether the same sample was measured repeatedly
- The statistical test(s) used AND whether they are one- or two-sided
Only common tests should be described solely by name; describe more complex techniques in the Methods section.
- A description of all covariates tested
- A description of any assumptions or corrections, such as tests of normality and adjustment for multiple comparisons
- A full description of the statistical parameters including central tendency (e.g. means) or other basic estimates (e.g. regression coefficient) AND variation (e.g. standard deviation) or associated estimates of uncertainty (e.g. confidence intervals)
- For null hypothesis testing, the test statistic (e.g. F , t , r) with confidence intervals, effect sizes, degrees of freedom and P value noted
Give P values as exact values whenever suitable.
- For Bayesian analysis, information on the choice of priors and Markov chain Monte Carlo settings
- For hierarchical and complex designs, identification of the appropriate level for tests and full reporting of outcomes
- Estimates of effect sizes (e.g. Cohen's d , Pearson's r), indicating how they were calculated

Our web collection on [statistics for biologists](#) contains articles on many of the points above.

Software and code

Policy information about [availability of computer code](#)

Data collection

Data analysis

For manuscripts utilizing custom algorithms or software that are central to the research but not yet described in published literature, software must be made available to editors and reviewers. We strongly encourage code deposition in a community repository (e.g. GitHub). See the Nature Portfolio [guidelines for submitting code & software](#) for further information.

Data

Policy information about [availability of data](#)

All manuscripts must include a [data availability statement](#). This statement should provide the following information, where applicable:

- Accession codes, unique identifiers, or web links for publicly available datasets
- A description of any restrictions on data availability
- For clinical datasets or third party data, please ensure that the statement adheres to our [policy](#)

The authors declare that all data supporting the findings of this study are available within the paper and its supplementary information files. The authors declare that all data supporting the findings of this study are available within the paper and its supplementary information files. Background maps for Figure 1 are Shuttle Radar Topography Mission Digital Elevation Model data at one arcsecond resolution from the NASA Land Processes Distributed Active Archive Center (<https://earthexplorer.usgs.gov/>); settlements, lakes and other features are from (<https://www.natureearthdata.com/>). Background image for the top left corner inset of Figure 1 from Google Earth and plate boundaries data courtesy of the U.S. Geological Survey.

Field-specific reporting

Please select the one below that is the best fit for your research. If you are not sure, read the appropriate sections before making your selection.

Life sciences Behavioural & social sciences Ecological, evolutionary & environmental sciences

For a reference copy of the document with all sections, see [nature.com/documents/nr-reporting-summary-flat.pdf](https://www.nature.com/documents/nr-reporting-summary-flat.pdf)

Ecological, evolutionary & environmental sciences study design

All studies must disclose on these points even when the disclosure is negative.

Study description	Geological sampling and geochemical characterisation of volcanic deposits of the Main Ethiopian Rift (MER)
Research sample	We sampled exclusively volcanic deposits mentioned in the literature that have been used to constrain the age of Omo I fossils. This includes tephra from Konso, Omo-Kibish, and Gademotta formations. We also sampled the previously described Qi2 eruption deposits of Shala volcano. Each sample was collected at its type section described in previous work, where the deposits are the most representative of each unit.
Sampling strategy	We sampled ~ 500g of material for each deposit in clean sample bags for Ar/Ar and geochemical analyses and repository. The quantity collected ensured to display enough grains for dating after cleaning (50-100 grains) and to conduct reproducible analyses of volcanic glass in the appropriate grain size section, i.e. 40-50 point analyses per sample, following international standards of tephrochronology work.
Data collection	At each site we described extensively the stratigraphy of the outcrops, measured the thickness of units and sampled deposits where best exposed and least altered. Tephra deposits were carefully sampled using a spatula or hammer (on indurated deposits) on cleaned and least altered outcrops. C. Vidal, C. Lane, A. Asrat, A. Deino, G. Yirgu, and A. Zafu collected the samples. C. Vidal, C. Lane, A. Deino and A. Zafu described the deposits (position, texture, thickness, color, grain size, alteration) and their environment and drew stratigraphic sections.
Timing and spatial scale	Fieldwork took place during the Ethiopian dry seasons (spring and autumn). Proximal samples for the Qi2 Shala eruption were sampled in May 2017 at Labusuka village, where it was previously described by Mohr et al. (1980) and where the exposure of the deposits is maximum in order to sample all units of the eruption. Tephra from Kibish and Konso were sampled in November 2018 during a second mission focused on sampling in southern Ethiopia. These were sampled at their type section, where exposure of the whole deposits is the best.
Data exclusions	No data was excluded in the sampling. Exclusion strategy for Ar/Ar dating: Following the approach of Kuiper et al. (2008, ref. 19) samples with low radiogenic yields ($40\text{Ar}^* < 10\%$, 23 grains), and obvious outliers (age > 1Ma, 6 grains) were rejected. Following this initial filtering, peak age distributions were defined by determining the youngest population of individual grain analyses ($n \geq 10$) that conforms to a Gaussian distribution with the expected scatter as indicated by the value of MSWD (Mean Square of Weighted Deviates); this second stage of filtering resulted in rejection of an additional ten older grains, leaving 71 accepted grains. Exclusion strategy for glass analyses: All geochemical datasets were initially reviewed to identify any clear outliers arising from either (i) accidental incorporation of a crystal inclusion in the glass analyses, or (ii) glass shards suffering unusually high alkali mobilisation / Na-loss, indicated by Na_2O values < 2 wt% and low totals < 91 wt%. Outlier removal was carried out conservatively to prevent accidental removal of shards that might represent true variability in magmatic composition. Marginal outliers were removed from plots, but have been left in Table S1 for completeness (marked as Discarded analyses).
Reproducibility	No experiment were conducted.
Randomization	Randomization is not applicable in the study of volcanic deposits
Blinding	Blinding is not applicable in the study of volcanic deposits
Did the study involve field work?	<input checked="" type="checkbox"/> Yes <input type="checkbox"/> No

Field work, collection and transport

Field conditions	Ethiopian Dry season (May 2017 and November 2018). The season was not relevant for the rock samples in particular but favoured the access to remote location by foot/car and bearable heat conditions.
Location	Shala Qi2 deposits in Labusuka (Site ETH17-14): Lat N 7.415018, Long E 38.456357 Konso (site ETH18-14): Lat N 5.41611, Long E 37.36317 Kibish KS type section (site ETH18-8): Lat N 5.34778, Long E 35.93684
Access & import/export	No permit is required for the collection a geological samples in Ethiopia. The sampling of Shala deposits was authorised by the School of Earth Sciences Addis Ababa University and the Oromiya Regional State (24 April 2017). Sampling at Konso and Kibish was permitted by the School of Earth Sciences Addis Ababa University and Ngangatom Woreda Local Administration (15 November 2018). Sample export was granted by the School of Earth Sciences, Addis Ababa University and FDRE Ministry of Mines, Petroleum and Natural Gas.

Disturbance

Sample collection caused no disturbance.
Local inhabitants gathered around during the description and sampling of the deposits and interacted with the team in a peaceful way. In more remote areas such as Konso, no disturbance was caused.

Reporting for specific materials, systems and methods

We require information from authors about some types of materials, experimental systems and methods used in many studies. Here, indicate whether each material, system or method listed is relevant to your study. If you are not sure if a list item applies to your research, read the appropriate section before selecting a response.

Materials & experimental systems

Methods

- | n/a | Involvement |
|-------------------------------------|--|
| <input checked="" type="checkbox"/> | <input type="checkbox"/> Antibodies |
| <input checked="" type="checkbox"/> | <input type="checkbox"/> Eukaryotic cell lines |
| <input checked="" type="checkbox"/> | <input type="checkbox"/> Palaeontology and archaeology |
| <input checked="" type="checkbox"/> | <input type="checkbox"/> Animals and other organisms |
| <input checked="" type="checkbox"/> | <input type="checkbox"/> Human research participants |
| <input checked="" type="checkbox"/> | <input type="checkbox"/> Clinical data |
| <input checked="" type="checkbox"/> | <input type="checkbox"/> Dual use research of concern |

- | n/a | Involvement |
|-------------------------------------|---|
| <input checked="" type="checkbox"/> | <input type="checkbox"/> ChIP-seq |
| <input checked="" type="checkbox"/> | <input type="checkbox"/> Flow cytometry |
| <input checked="" type="checkbox"/> | <input type="checkbox"/> MRI-based neuroimaging |